

Measurement of $B \rightarrow D^{(*)}\tau\nu$ using full reconstruction tags

I. Adachi, H. Fujii, J. Haba, T. Hara, M. Hazumi, T. Higuchi, Y. Igarashi, R. Itoh, Y. Iwasaki, N. Katayama, A. Kibayashi, H. Kichimi, P. Krokovny, J. MacNaughton, I. Nakamura, M. Nakao, S. Nishida, T. Nozaki, H. Ozaki, Y. Sakai, J. Schümann, K. Sumisawa, S. Y. Suzuki, F. Takasaki, M. Tanaka, N. Taniguchi, K. Trabelsi, T. Tsuboyama, S. Uehara, S. Uno, Y. Ushiroda, J. Wicht, and M. Yamauchi
High Energy Accelerator Research Organization (KEK), Tsukuba

H. Aihara, N. C. Hastings, K. Itoh, M. Iwasaki, H. Kakuno, A. Kusaka, Y. Nakahama, H. Nakayama, and K. Tanabe
Department of Physics, University of Tokyo, Tokyo

K. Arinstein, V. Aulchenko, I. Bedny, A. Bondar, S. Eidelman, D. Epifanov, N. Gabyshev, A. Garmash, A. Kuzmin, A. Poluektov, V. Shebalin, B. Shwartz, Y. Usov, A. Vinokurova, V. Zhilich, V. Zhulanov, and O. Zyukova
Budker Institute of Nuclear Physics, Novosibirsk and Novosibirsk State University, Novosibirsk

T. Aso
Toyama National College of Maritime Technology, Toyama

T. Aushev
École Polytechnique Fédérale de Lausanne (EPFL), Lausanne and Institute for Theoretical and Experimental Physics, Moscow

T. Aziz, A. Das, G. Gokhroo, and N. J. Joshi
Tata Institute of Fundamental Research, Mumbai

S. Bahinipati, A. Drutskoy, P. Goldenzweig, K. Kinoshita, and A. J. Schwartz
University of Cincinnati, Cincinnati, Ohio 45221

A. M. Bakich, S. McOnie, L. S. Peak, K. E. Varvell, and B. D. Yabsley
School of Physics, University of Sydney, NSW 2006

V. Balagura, R. Chistov, M. Danilov, D. Liventsev, T. Medvedeva, R. Mizuk, P. Pakhlov, G. Pakhlova, E. Solovieva, I. Tikhomirov, and T. Uglov
Institute for Theoretical and Experimental Physics, Moscow

Y. Ban and J. Wang
Peking University, Beijing

E. Barberio, T. Julius, A. Limosani, M. E. Sevier, G. N. Taylor, Y. F. Tse, P. Urquijo, and R. Wedd

University of Melbourne, School of Physics, Victoria 3010

A. Bay, R. Louvot, O. Schneider, K. Vervink, and N. Zwahlen
École Polytechnique Fédérale de Lausanne (EPFL), Lausanne

K. Belous, M. Shapkin, and A. Sokolov
Institute of High Energy Physics, Protvino

V. Bhardwaj, R. Kumar, and J. B. Singh
Panjab University, Chandigarh

B. Bhuyan
India Institute of Technology Guwahati, Guwahati

M. Bischofberger, M. Fujikawa, H. Hayashii, K. Miyabayashi, S. Noguchi, and A. Sekiya
Nara Women's University, Nara

S. Blyth and C. H. Wang
National United University, Miao Li

A. Bozek, J. Brodzicka, P. Kapusta, A. Matyja, Z. Natkaniec,
W. Ostrowicz, H. Palka, M. Rozanska, J. Stypula, and J. Wiechczynski
H. Niewodniczanski Institute of Nuclear Physics, Krakow

M. Bračko and S. Korpar
*University of Maribor, Maribor and
J. Stefan Institute, Ljubljana*

T. E. Browder, M. Jones, J. Li, K. Nishimura,
M. Peters, H. Sahoo, C. P. Shen, and G. Varner
University of Hawaii, Honolulu, Hawaii 96822

M.-C. Chang
Department of Physics, Fu Jen Catholic University, Taipei

P. Chang, Y.-W. Chang, Y. Chao, K.-F. Chen, P.-Y. Chen, C.-C. Chiang, W.-S. Hou,
Y. B. Hsiung, S.-W. Lin, J.-G. Shiu, K. Ueno, C. C. Wang, M.-Z. Wang, and J.-T. Wei
Department of Physics, National Taiwan University, Taipei

A. Chen and H. Nakazawa
National Central University, Chung-li

B. G. Cheon and Y. Unno
Hanyang University, Seoul

I.-S. Cho, J. H. Kang, Y.-J. Kwon, and S.-H. Kyeong
Yonsei University, Seoul

S.-K. Choi

Gyeongsang National University, Chinju

Y. Choi, J. H. Kim, C. W. Park, and K. S. Park

Sungkyunkwan University, Suwon

J. Crnkovic

University of Illinois at Urbana-Champaign, Urbana, Illinois 61801

J. Dalseno, A. Moll, K. Prothmann, and F. Simon

*Max-Planck-Institut für Physik, München and
Excellence Cluster Universe, Technische Universität München, Garching*

M. Dash, L. E. Pilonen, and Y. Yusa

IPNAS, Virginia Polytechnic Institute and State University, Blacksburg, Virginia 24061

W. Dungel, G. Leder, F. Mandl, M. Pernicka, C. Schwanda, and L. Widhalm

Institute of High Energy Physics, Vienna

M. Feindt, M. Kreps, T. Kuhr, T. Müller, and S. Neubauer

Institut für Experimentelle Kernphysik, Universität Karlsruhe, Karlsruhe

B. Golob and P. Kržan

*Faculty of Mathematics and Physics,
University of Ljubljana, Ljubljana and
J. Stefan Institute, Ljubljana*

M. Grosse Perdekamp

*University of Illinois at Urbana-Champaign, Urbana, Illinois 61801 and
RIKEN BNL Research Center, Upton, New York 11973*

H. Guo, C. Liu, L. M. Zhang, and Z. P. Zhang

University of Science and Technology of China, Hefei

H. Ha, B.-Y. Han, B. R. Ko, S.-H. Lee, and E. Won

Korea University, Seoul

K. Hara, K. Hayasaka, T. Iijima, K. Inami, T. Jinno, Y. Miyazaki,

T. Mori, T. Ohshima, K. Senyo, S. Shiizuka, Y. Suzuki, and K. Tsunada
Nagoya University, Nagoya

Y. Hasegawa

Shinshu University, Nagano

D. Heffernan, Y. Kuroki, H. Miyake, and S. Shinomiya

Osaka University, Osaka

Y. Horii, Y. Mikami, T. Nagamine, P. Schönmeier, and H. Yamamoto
Tohoku University, Sendai

Y. Hoshi and K. Neichi
Tohoku Gakuin University, Tagajo

K. Hoshina and O. Nitoh
Tokyo University of Agriculture and Technology, Tokyo

H. J. Hyun, D. H. Kah, H. J. Kim, H. O. Kim, Y. I. Kim, H. Park, and H. K. Park
Kyungpook National University, Taegu

A. Ishikawa, A. Sugiyama, and S. Suzuki
Saga University, Saga

H. Ishino*
Tokyo Institute of Technology, Tokyo

M. Iwabuchi, Y. J. Kim, and Y. Uchida
The Graduate University for Advanced Studies, Hayama

S. U. Kataoka
Nara University of Education, Nara

H. Kawai and E. Kurihara
Chiba University, Chiba

T. Kawasaki, H. Miyata, K. Sakai, N. Tamura, and M. Watanabe
Niigata University, Niigata

C. Kiesling and B. Riesert
Max-Planck-Institut für Physik, München

S. K. Kim, M. J. Lee, S. E. Lee, and S. L. Olsen
Seoul National University, Seoul

T. Kumita, E. Kuroda, T. Sumiyoshi, and Y. Ueki
Tokyo Metropolitan University, Tokyo

J. S. Lange
Justus-Liebig-Universität Gießen, Gießen

D. Marlow
Princeton University, Princeton, New Jersey 08544

R. Mussa
INFN - Sezione di Torino, Torino

Y. Nagasaka
Hiroshima Institute of Technology, Hiroshima

E. Nakano and Y. Teramoto
Osaka City University, Osaka

A. Ogawa and R. Seidl
RIKEN BNL Research Center, Upton, New York 11973

S. Ogawa and H. Shibuya
Toho University, Funabashi

S. Okuno and Y. Watanabe
Kanagawa University, Yokohama

R. Pestotnik, M. Starič, T. Zivko, and A. Zupanc
J. Stefan Institute, Ljubljana

N. Sasao
Kyoto University, Kyoto

L. Shang, P. Wang, X. L. Wang, C. Z. Yuan, and C. C. Zhang
Institute of High Energy Physics, Chinese Academy of Sciences, Beijing

R. Sinha
Institute of Mathematical Sciences, Chennai

S. Stanič
University of Nova Gorica, Nova Gorica

Y. Yamashita
Nippon Dental University, Niigata

Abstract

We present measurements of $B \rightarrow D^* \tau \nu$ and $B \rightarrow D \tau \nu$ decays using 604.5 fb^{-1} of data collected at the $\Upsilon(4S)$ resonance with the Belle detector at the KEKB asymmetric-energy e^+e^- collider. Events are tagged by fully reconstructing one of the B mesons in hadronic modes. We obtain $\mathcal{B}(B^+ \rightarrow \bar{D}^0 \tau^+ \nu) = (1.51^{+0.41}_{-0.39} {}^{+0.24}_{-0.19} \pm 0.15)\%$, $\mathcal{B}(B^+ \rightarrow \bar{D}^{*0} \tau^+ \nu) = (3.04^{+0.69}_{-0.66} {}^{+0.40}_{-0.47} \pm 0.22)\%$, $\mathcal{B}(B^0 \rightarrow D^- \tau^+ \nu) = (1.01^{+0.46}_{-0.41} {}^{+0.13}_{-0.11} \pm 0.10)\%$, $\mathcal{B}(B^0 \rightarrow D^{*-} \tau^+ \nu) = (2.56^{+0.75}_{-0.66} {}^{+0.31}_{-0.22} \pm 0.10)\%$ where the first error is statistical, the second is systematic, and the third is due to the uncertainty in the branching fraction for the normalization mode.

*now at Okayama University, Okayama

1. INTRODUCTION

The semileptonic B decay to τ channel, $B \rightarrow D^{(*)}\tau\nu$, is a sensitive probe of extensions to the Standard Model (SM). In the SM, it occurs via an external W emission diagram with predicted branching fractions of $(0.69 \pm 0.04)\%$ and $(1.41 \pm 0.07)\%$ for the $B^0 \rightarrow D^-\tau^+\nu_\tau$ and $B^0 \rightarrow D^{*-}\tau^+\nu_\tau$ modes, respectively [1]. On the other hand, in extensions of the SM, such as the Two Higgs Doublet Models (2HDM) and the Minimal Supersymmetric Standard Model (MSSM), a charged Higgs boson (H^\pm) may contribute to the decay amplitude at tree level, and the branching fraction may be modified significantly [2, 3, 4, 5, 6]. Both $B \rightarrow D^{(*)}\tau\nu$ and the purely leptonic decay $B^+ \rightarrow \tau^+\nu_\tau$ have similar sensitivity to H^\pm bosons with different theoretical systematics; the former suffers from uncertainty in the form factor, while the latter requires knowledge of the B decay constant f_B . Therefore, the two decays provide complementary approaches to searching for H^\pm signatures in B decays.

Experimentally, measurements of the $B \rightarrow D^{(*)}\tau\nu$ decays are challenging because at least two neutrinos are present in the final state. The Belle collaboration has previously reported the first observation of the decay $B^0 \rightarrow D^{*-}\tau^+\nu$, by inclusively reconstructing the accompanying B via a 4-vector sum of all the charged and neutral tracks other than the D^* and τ daughter track candidates. The reported branching fraction is $\mathcal{B}(B^0 \rightarrow D^{*-}\tau^+\nu) = (2.02^{+0.40}_{-0.37}(\text{stat}) \pm 0.37(\text{syst}))\%$ [7]. In this paper, we present new measurements of $B^0 \rightarrow D^{(*)-}\tau^+\nu$ and $B^+ \rightarrow \overline{D}^{(*)0}\tau^+\nu$ decays. Here we fully reconstruct one of the B mesons in the event, referred to hereafter as the tag side (B_{tag}), and compare properties of the remaining particles, referred to as the signal side (B_{sig}), to those expected for signal and background. The method allows us to strongly suppress the combinatorial backgrounds, and correctly calculate the missing mass which discriminates the signal from $B \rightarrow D^{(*)}\ell\nu$ background. Using a similar technique, the BaBar collaboration has reported the branching fractions, $\mathcal{B}(B^0 \rightarrow D^-\tau^+\nu) = (0.86 \pm 0.24 \pm 0.11 \pm 0.06)\%$ and $\mathcal{B}(B^0 \rightarrow D^{*-}\tau^+\nu) = (1.62 \pm 0.31 \pm 0.10 \pm 0.05)\%$, where the third uncertainty is from the normalization mode. They also measured distributions of the lepton momentum and the squared momentum transfer [8].

In order to avoid experimental bias, the signal region in data is blinded until the event selection criteria are finalized. Inclusion of the charge conjugate decays is implied throughout this paper.

2. EXPERIMENT AND DATA SET

The analysis is based on the data recorded with the Belle detector at the KEKB e^+e^- asymmetric-energy collider operating at the center-of-mass (c.m.) energy of the $\Upsilon(4S)$ resonance. KEKB consists of a low energy ring (LER) of 3.5 GeV positrons and a high energy ring (HER) of 8 GeV electrons [9]. The $\Upsilon(4S)$ data set used in this analysis corresponds to an integrated luminosity of 605 fb^{-1} and contains 657×10^6 $B\overline{B}$ events.

The Belle detector is a large-solid-angle magnetic spectrometer that consists of a silicon vertex detector (SVD), a 50-layer central drift chamber (CDC), an array of aerogel threshold Cherenkov counters (ACC), a barrel-like arrangement of time-of-flight scintillation counters (TOF), and an electromagnetic calorimeter (ECL) comprised of CsI(Tl) crystals located inside a super-conducting solenoid coil that provides a 1.5 T magnetic

field. Muons and K_L^0 mesons are identified by arrays of resistive plate counters interspersed in the iron yoke (KLM). The detector is described in detail elsewhere [10].

A detailed Monte Carlo (MC) simulation, based on the GEANT package [11], is used to estimate the signal detection efficiency and to study the background. Large samples of the signal decays are generated with the EVTGEN package [12] using the ISGW II form factor model [13]. To model the $B\bar{B}$ and $q\bar{q}$ ($q = u, d, s, c$) backgrounds, large generic $B\bar{B}$ and $q\bar{q}$ MC samples, corresponding to about twice the integrated luminosity of data are used. To further increase the $B\bar{B}$ MC statistics, we also use special $B\bar{B}$ MC samples, corresponding to 1.5×10^{10} $B^0\bar{B}^0$ and B^+B^- pairs, where events are filtered based on event generator information before running the time consuming GEANT detector simulation.

3. EVENT RECONSTRUCTION AND SELECTION

3.1. Tag-side Reconstruction

Charged particle tracks are reconstructed from hits in the SVD and CDC. They are required to satisfy track quality cuts based on their impact parameters relative to the measured profile of the interaction point (IP) of the two beams. Charged kaons are identified by combining information on ionization loss (dE/dx) in the CDC, Cherenkov light yields in the ACC and time-of-flight measured by the TOF system. For the nominal requirement, the kaon identification efficiency is approximately 88% and the probability of misidentifying a pion as a kaon is about 8%. Hadron tracks that are not identified as kaons are treated as pions. Tracks satisfying the lepton identification criteria, as described below, are removed from consideration. Electron identification is based on a combination of dE/dx in CDC, the response of the ACC, shower shape in the ECL, position matching between ECL clusters and the track, and the ratio of the energy deposited in the ECL to the momentum measured by the tracking system. Muon candidates are selected using range of tracks measured in KLM and the deviation of hits from the extrapolated track trajectories. The lepton identification efficiencies are estimated to be about 90% for both electrons and muons in the momentum region above $1.2 \text{ GeV}/c$. The hadron misidentification rate is measured using reconstructed $K_S^0 \rightarrow \pi^+\pi^-$ decays and found to be less than 0.2% for electrons and 1.5% for muons in the same momentum region. K_S^0 mesons are reconstructed using pairs of charged tracks that have an invariant mass within $\pm 30 \text{ MeV}/c^2$ of the known K_S^0 mass and a well reconstructed vertex that is displaced from the IP. Candidate γ 's are required to have a minimum energy deposit $E_\gamma \geq 50 \text{ MeV}$. Candidate π^0 mesons are reconstructed using $\gamma\gamma$ pairs with invariant masses between 117 and $150 \text{ MeV}/c^2$. For slow π^0 's used in D^* reconstruction, the minimum γ energy requirement is lowered to 30 MeV .

B_{tag} candidates are reconstructed in the following decay modes: $B^+ \rightarrow \bar{D}^{(*)0}\pi^+$, $\bar{D}^{(*)0}\rho^+$, $\bar{D}^{(*)0}a_1^+$, $\bar{D}^{(*)0}D_s^{(*)+}$, and $B^0 \rightarrow D^{(*)-}\pi^+$, $D^{(*)-}\rho^+$, $D^{(*)-}a_1^+$, $D^{(*)-}D_s^{(*)+}$. Candidate ρ^+ and ρ^0 mesons are reconstructed in the $\pi^+\pi^0$ and $\pi^+\pi^-$ decay modes, by requiring their invariant masses to be within $\pm 225 \text{ MeV}/c^2$ of the nominal ρ mass. We then select a_1^+ candidates by combining a ρ^0 candidate and a pion with invariant mass between 0.7 and $1.6 \text{ GeV}/c^2$ and require that the charged tracks form a good vertex. D meson candidates are reconstructed in the following decay modes: $\bar{D}^0 \rightarrow K^+\pi^-$, $K^+\pi^-\pi^0$, $K^+\pi^-\pi^+\pi^-$, $K_S^0\pi^0$, $K_S^0\pi^-\pi^+$, $K_S^0\pi^-\pi^+\pi^0$, K^-K^+ , and $D^- \rightarrow K^+\pi^-\pi^-$, $K^+\pi^-\pi^-\pi^0$, $K_S^0\pi^-$, $K_S^0\pi^-\pi^0$,

$K_S^0\pi^+\pi^-\pi^-$, $K^+K^-\pi^-$, $D_s^+ \rightarrow K_S^0K^+$, $K^+K^-\pi^+$. The D candidates are required to have an invariant mass M_D within $4 - 5\sigma$ (σ is the mass resolution) of the nominal D mass value depending on the mode. D^* mesons are reconstructed as $D^{*+} \rightarrow D^0\pi^+$, $D^+\pi^0$, $D^{*0} \rightarrow D^0\pi^0$, $D^0\gamma$, and $D_s^{*+} \rightarrow D_s^+\gamma$. D^* candidates from modes that include a pion are required to have a mass difference $\Delta M = M_{D\pi} - M_D$ within $\pm 5 \text{ MeV}/c^2$ of its nominal value. For decays with a photon, we require that the mass difference $\Delta M = M_{D\gamma} - M_D$ be within $\pm 20 \text{ MeV}/c^2$ of the nominal value.

The selection of B_{tag} candidates is based on the beam-constrained mass $M_{\text{bc}} \equiv \sqrt{E_{\text{beam}}^2 - p_B^2}$ and the energy difference $\Delta E \equiv E_B - E_{\text{beam}}$. Here, E_B and p_B are the reconstructed energy and momentum of the B_{tag} candidate in the e^+e^- c.m. system, and E_{beam} is the beam energy in the c.m. frame. The background from jet-like continuum events ($e^+e^- \rightarrow q\bar{q}$, $q = u, d, s, c$) is suppressed on the basis of event topology: we require the normalized second Fox-Wolfram moment (R_2) [14] to be smaller than 0.5, and $|\cos\theta_{\text{th}}| < 0.8$, where θ_{th} is the angle between the thrust axis of the B candidate and that of the remaining tracks in the event. The latter requirement is not applied to $B^+ \rightarrow \bar{D}^0\pi^+$, $\bar{D}^{*0}(\rightarrow \bar{D}^0\pi^0)\pi^+$ and $B^0 \rightarrow D^{*-}(\rightarrow \bar{D}^0\pi^-)\pi^+$ decays, where the continuum background is small. For the B_{tag} candidate, we require $5.27 \text{ GeV}/c^2 < M_{\text{bc}} < 5.29 \text{ GeV}/c^2$ and $-80 \text{ MeV} < \Delta E < 60 \text{ MeV}$. If an event has multiple B_{tag} candidates, we choose the one having the smallest χ^2 based on deviations from the nominal values of ΔE , the D candidate mass, and the $D^* - D$ mass difference if applicable. The number of B^+ and B^0 candidates in the selected region are 1.75×10^6 and 1.18×10^6 , respectively. By fitting the distribution to the sum of an empirical parameterization of the background shape [15] and a signal shape [16], we estimate that in the selected region there are $(10.11 \pm 0.03) \times 10^5$ (with purity=0.58) B^+ and $(6.05 \pm 0.03) \times 10^5$ (with purity=0.51) B^0 events, respectively.

3.2. Signal-side Reconstruction

In the events where a B_{tag} is reconstructed, we search for decays of B_{sig} into a $D^{(*)}$, τ and a neutrino. In the present analysis, the τ lepton is identified in the leptonic decay modes, $\mu^-\bar{\nu}\nu$ and $e^-\bar{\nu}\nu$. We require that the charge/flavor of the τ daughter particles and the D meson are consistent with the B_{sig} flavor, opposite to the B_{tag} flavor. The loss of signal due to $B^0 - \bar{B}^0$ mixing is estimated by the MC simulation.

The procedures to reconstruct charged particles ($e^\pm, \mu^\pm, \pi^\pm, K^\pm$) and neutral particles (π^0, K_S^0) for the signal side are the same as those used for the tag side. For γ candidates, we require a minimum energy threshold of 50 MeV for the barrel, and 100 (150) MeV for the forward (backward) end-cap ECL. A higher threshold is used for the endcap ECL, where the effect of beam background is more severe. We also require that the lepton momentum in the laboratory frame exceeds $0.6 \text{ GeV}/c$ to ensure good lepton identification efficiency.

The decay modes used for D reconstruction are slightly different from those used for the tagging side: $\bar{D}^0 \rightarrow K^+\pi^-$, $K^+\pi^-\pi^0$, $K^+\pi^-\pi^+\pi^-$, $K^+\pi^-\pi^+\pi^-\pi^0$, $K_S^0\pi^0$, $K_S^0\pi^-\pi^+$, $K_S^0\pi^-\pi^+\pi^0$, and $D^- \rightarrow K^+\pi^-\pi^-$, $K^+\pi^-\pi^-\pi^0$, $K_S^0\pi^-$. The D candidates are required to have an invariant mass M_D within 5σ of the nominal D mass value. D^* mesons are reconstructed using the same decay modes as on the tagging side: $D^{*+} \rightarrow D^0\pi^+$, $D^+\pi^0$, and $D^{*0} \rightarrow D^0\pi^0$, $D^0\gamma$. D^* candidates are required to have a mass difference $\Delta M = M_{D\pi(\gamma)} - M_D$ within 5σ of the nominal value.

For signal selection, we use the following variables that characterize the signal decay: the missing mass squared in the event (M_{miss}^2), the momentum (in the c.m. system) of the τ daughter leptons (P_ℓ^*), and the extra energy in the ECL ($E_{\text{extra}}^{\text{ECL}}$). The missing mass squared is calculated as $M_{\text{miss}}^2 = (E_{B_{\text{tag}}} - E_D - E_{\tau \rightarrow X})^2 - (-\vec{P}_{B_{\text{tag}}} - \vec{P}_{D^{(*)}} - \vec{P}_{\tau \rightarrow X})^2$, using the energy and momenta of the B_{tag} , the $D^{(*)}$ candidate and the lepton from the τ decay. The signal decay is characterized by large M_{miss}^2 due to the presence of more than two neutrinos in the final state. The lepton momenta (P_ℓ^*) distribute lower than those from primary B decays. The extra energy in the ECL ($E_{\text{extra}}^{\text{ECL}}$) is the sum of the energies of photons that are not associated with either the B_{tag} or the B_{sig} reconstruction. ECL clusters with energies greater than 50 MeV in the barrel, and 100 (150) MeV in the forward (backward) end-cap ECL are used to calculate $E_{\text{extra}}^{\text{ECL}}$. For signal events, $E_{\text{extra}}^{\text{ECL}}$ must be either zero or a small value arising from beam background hits, therefore, signal events peak at low $E_{\text{extra}}^{\text{ECL}}$. On the other hand, background events are distributed toward higher $E_{\text{extra}}^{\text{ECL}}$ due to the contribution from additional neutral clusters. We also require that the event has no extra charged tracks and no π^0 candidate other than those from the signal decay and those used in the B_{tag} reconstruction. Table I summarizes the cuts to define the signal region. The cuts are optimized by maximizing the figure of merit (F.O.M.), defined as $\text{F.O.M.} = N_S / \sqrt{N_S + N_B}$, where $N_S(N_B)$ are the number of signal (total background) events in the signal region, assuming the SM branching fractions for the $D\tau\nu$ and the $D^*\tau\nu$ modes.

Cut variable	$B \rightarrow \bar{D}^0(D^-)\tau^+\nu$	$B \rightarrow \bar{D}^{*0}(D^{*-})\tau^+\nu$
Number of extra tracks	= 0	= 0
Number of extra π^0	= 0	= 0
P_ℓ^*	$\leq 1.2 \text{ GeV}/c$	$\leq 1.2 \text{ GeV}/c$
M_{miss}^2	$\geq 2.0 \text{ GeV}^2/c^4$	$\geq 1.6 \text{ GeV}^2/c^4$
$E_{\text{extra}}^{\text{ECL}}$	$\leq 0.2 \text{ GeV}$	$\leq 0.2 \text{ GeV}$

TABLE I: Summary of the signal selection criteria.

3.3. Signal Detection Efficiency and Expected Background

Table II lists the signal detection efficiencies, which are estimated from signal MC simulation, with the selection criteria shown in Table I. Taking account of the cross talks between $B \rightarrow D\tau\nu$ and $B \rightarrow D^*\tau\nu$ modes, the signal detection efficiency (ϵ_{ij}) is defined as,

$$N_{ij} = \epsilon_{ij} \cdot \mathcal{B}_j \cdot N_{\text{tag}} \quad , \quad (1)$$

where N_{ij} represents the yield of the generated j -th mode reconstructed in the i -th mode. \mathcal{B}_j is the branching fraction of the j -th mode including the sub-decay (τ and $D^{(*)}$) branching fractions. N_{tag} is the number of B events fully reconstructed on the tagging side. Table II also shows, in parentheses, the efficiencies without cuts on M_{miss}^2 and $E_{\text{extra}}^{\text{ECL}}$. These are the two variables used to extract the signal yields.

Recon'd mode	Generated modes	
	$\overline{D}^0\tau^+\nu$	$\overline{D}^{*0}\tau^+\nu$
$\overline{D}^0\tau^+\nu$	2.55 ± 0.05 (4.87 ± 0.08)	0.90 ± 0.05 (1.75 ± 0.07)
$\overline{D}^{*0}\tau^+\nu$	0.34 ± 0.01 (1.33 ± 0.02)	1.08 ± 0.03 (2.11 ± 0.04)

Recon'd mode	Generated modes	
	$D^-\tau^+\nu$	$D^{*-}\tau^+\nu$
$D^-\tau^+\nu$	3.21 ± 0.06 (6.86 ± 0.09)	0.23 ± 0.03 (0.55 ± 0.03)
$D^{*-}\tau^+\nu$	0.11 ± 0.01 (0.27 ± 0.01)	0.80 ± 0.02 (1.54 ± 0.03)

TABLE II: Signal detection efficiency (%) matrix for B^+ (top) and B^0 (bottom) modes. The values in parenthesis are the efficiencies without cuts on M_{miss}^2 and $E_{\text{extra}}^{\text{ECL}}$.

According to the MC simulation, the expected number of signal (background) events in the signal region is 19(48) for $B^+ \rightarrow \overline{D}^0\tau^+\nu$, 7(13) for $B^0 \rightarrow D^-\tau^+\nu$, 18(25) for $B^+ \rightarrow \overline{D}^{*0}\tau^+\nu$, and 7(6) for $B^0 \rightarrow D^{*-}\tau^+\nu$. The major background sources are semileptonic B decays, $B \rightarrow D\ell\nu$, $D^*\ell\nu$ and $D^{**}\ell\nu$ (60-70% depending on the decay mode). The remaining background comes from hadronic B decays including a D meson in the final state. Background from $q\bar{q}$ processes are found to be small (less than one event). As shown in Table II, the cross talk between $B \rightarrow D\tau\nu$ and $B \rightarrow D^*\tau\nu$ arises, when a pion or a photon is missed in the reconstruction of D^* , or when a random photon is combined with a D to form a fake D^* . The cross-feed to other B^0 or B^+ tag samples is negligibly small.

4. CALIBRATION USING THE $B \rightarrow D^{(*)}\ell\nu$ SAMPLE

We use $B \rightarrow D^{(*)}\ell\nu$ ($\ell = e/\mu$) decays as control samples to calibrate the background MC simulation and to verify the $E_{\text{extra}}^{\text{ECL}}$ simulation. We also use these decays to normalize the extracted signal yields. We select $B \rightarrow D^{(*)}\ell\nu$ decays using the same selection requirements as $B \rightarrow D^{(*)}\tau\nu$, but without the cut on the momentum of the τ daughter lepton and with $|M_{\text{mis}}^2| < 1 \text{ GeV}^2/c^4$ and $E_{\text{extra}}^{\text{ECL}} < 1.2 \text{ GeV}$. The four calibration decay modes: $B^+ \rightarrow \overline{D}^0\ell^+\nu$, $B^+ \rightarrow \overline{D}^{*0}\ell^+\nu$, $B^0 \rightarrow D^-\ell^+\nu$, and $B^0 \rightarrow D^{*-}\ell^+\nu$, peak around zero in the missing mass distributions, as shown in Figure 1.

The yields of the calibration modes are extracted by fitting the distributions with expected shapes based on MC simulation for the signal and the background. The major background in each distribution arises from other semileptonic decays, where a pion or a photon is missed (i.e. $B \rightarrow D^*\ell\nu$ is reconstructed as $B \rightarrow D\ell\nu$ if the soft π^0 or γ from the D^* is missed), or a random photon is used in D^{*0} reconstruction (i.e. $B \rightarrow D\ell\nu$ misreconstructed as $B \rightarrow D^*\ell\nu$). Here the two distributions for B^+ and B^0 candidates are fitted simultaneously. Table III lists the yields extracted for each calibration decay mode, which include the yields detected as cross talk; for example, the yield of $\overline{D}^0\ell^+\nu$ is the sum of $B^+ \rightarrow \overline{D}^0\ell^+\nu$ decays measured in the $\overline{D}^0\ell^+\nu$ and $\overline{D}^{*0}\ell^+\nu$ distributions. When we compare the extracted yields with expected yields from the MC simulation, the ratio

of the measured to the expected yields (R_{corr}) are found to be 0.75 – 0.84, depending on the mode. The ratios are used as scale factors to correct the normalization in the MC simulation for $B \rightarrow D^{(*)}\ell\nu$ semileptonic decays, which are the major backgrounds in the $B \rightarrow D^{(*)}\tau\nu$ detection.

	$\overline{D}^0\ell^+\nu$	$\overline{D}^{*0}\ell^+\nu$	$\overline{D}^-\ell^+\nu$	$\overline{D}^{*-}\ell^+\nu$
Yield	1156 ± 44	2152 ± 76	338 ± 21	769 ± 35
Efficiency (%)	8.97 ± 0.05	6.86 ± 0.08	11.3 ± 0.12	5.43 ± 0.04

TABLE III: Yields and efficiencies of the calibration modes.

Figure 2 compares the $E_{\text{extra}}^{\text{ECL}}$ distribution for the control samples in data and the MC simulation after the correction. The agreement between the data and the MC simulation is satisfactory, and valid the $E_{\text{extra}}^{\text{ECL}}$ simulation. We also confirm that the number of events found in the sideband of the $(M_{\text{miss}}^2, E_{\text{extra}}^{\text{ECL}})$ signal region is consistent within statistics for the data and the scaled MC simulation. Here the sideband is defined by $E_{\text{extra}}^{\text{ECL}} > 0.4 \text{ GeV}$, and $M_{\text{miss}}^2 < 1.0 \text{ GeV}^2/c^4$, for all four signal modes.

5. SIGNAL EXTRACTION

The $B \rightarrow D\tau\nu$ and $B \rightarrow D^*\tau\nu$ signal yields are extracted using unbinned extended maximum likelihood fits to the two-dimensional $(M_{\text{miss}}^2, E_{\text{extra}}^{\text{ECL}})$ distributions obtained after the selection of the signal decays. The fit components are two signal modes; $B \rightarrow D\tau\nu$ and $B \rightarrow D^*\tau\nu$, and the backgrounds from $B \rightarrow D\ell\nu$, $B \rightarrow D^*\ell\nu$ and other processes. The likelihood is constructed as,

$$L = \frac{e^{-\sum_j N_j}}{N!} \prod_{i=1}^N F(M_{\text{miss}}^2, E_{\text{extra}}^{\text{ECL}}) \quad , \quad (2)$$

where

$$\begin{aligned} F(M_{\text{miss}}^2, E_{\text{extra}}^{\text{ECL}}) &= N_{D\tau\nu} f_{D\tau\nu}(M_{\text{miss}}^2, E_{\text{extra}}^{\text{ECL}}) + N_{D^*\tau\nu} f_{D^*\tau\nu}(M_{\text{miss}}^2, E_{\text{extra}}^{\text{ECL}}) \\ &+ N_{D\ell\nu} f_{D\ell\nu}(M_{\text{miss}}^2, E_{\text{extra}}^{\text{ECL}}) + N_{D^*\ell\nu} f_{D^*\ell\nu}(M_{\text{miss}}^2, E_{\text{extra}}^{\text{ECL}}) \\ &+ N_{\text{other}} f_{\text{other}}(M_{\text{miss}}^2, E_{\text{extra}}^{\text{ECL}}) \quad . \end{aligned} \quad (3)$$

Here N_j and $f_j(M_{\text{miss}}^2, E_{\text{extra}}^{\text{ECL}})$ represent the number of events and the two-dimensional probability density function (PDF) as a function of M_{miss}^2 and $E_{\text{extra}}^{\text{ECL}}$, respectively, for process j . In the fit to the $B^0 \rightarrow D^{*-}\tau^+\nu$ distribution, the $D\tau\nu$ cross-feed ($f_{D\tau\nu}$) and $D\ell\nu$ background ($f_{D\ell\nu}$) are not included, because their contribution are found to be small according to the MC simulation. The fit region is defined by $(-2 \text{ GeV}^2/c^4 < M_{\text{miss}}^2 < 8 \text{ GeV}^2/c^4, 0 \text{ GeV} < E_{\text{extra}}^{\text{ECL}} < 1.2 \text{ GeV})$ for all four signal modes.

The two-dimensional PDF's for $D^{(*)}\tau\nu$ and $D^{(*)}\ell\nu$ processes are obtained by taking the product of a one-dimensional PDF for each variable, as the correlations between M_{miss}^2 and $E_{\text{extra}}^{\text{ECL}}$ are found to be small in the MC simulation. The one-dimensional PDF's for M_{miss}^2 are modeled by asymmetric Gaussian or double Gaussian distributions,

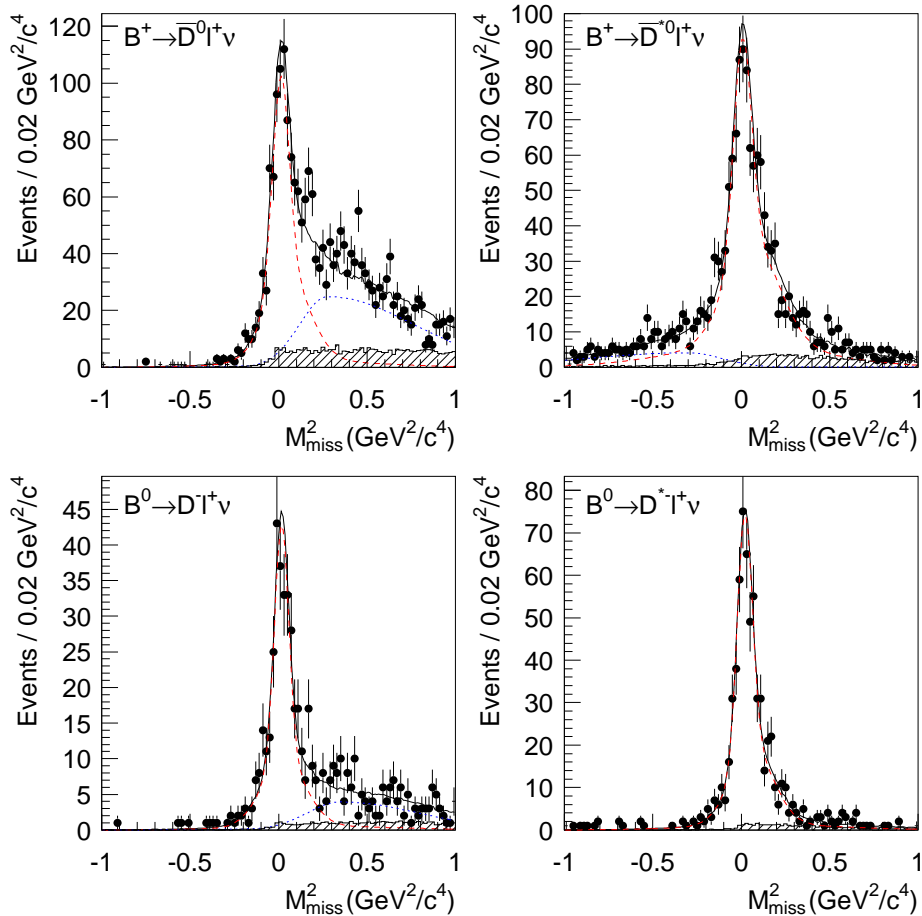


FIG. 1: Distribution of missing mass squared (M_{miss}^2) for $B^+ \rightarrow \bar{D}^0 \ell^+ \nu$ (top-left), $B^+ \rightarrow \bar{D}^{*0} \ell^+ \nu$ (top-right), $B^0 \rightarrow D^- \ell^+ \nu$ (bottom-left), and $B^0 \rightarrow D^{*-} \ell^+ \nu$ (bottom-right). Data are plotted as points with error bars, the results of the fit (solid line) along with the signal (dashed red line), other semileptonic decays (dotted blue line) and misidentified hadronic events (hatched histogram) components are also shown.

whereas the PDF's for $E_{\text{extra}}^{\text{ECL}}$ are histograms obtained from the MC simulation. The PDF for other background processes (f_{other}) uses the two-dimensional histograms obtained from MC simulation, since correlations between the two variables are significant for these background processes, which mainly come from hadronic B decays.

We fit the distributions for B^0 and B^+ tags separately. The cross talk between the two tags is found to be small according to the MC simulation. For each B^0 and B^+ tag, we then fit simultaneously the two distributions for the $D\tau\nu$ and $D^*\tau\nu$ components. The ratio of the number of events found in the two distributions is constrained according to the efficiency matrix shown in Table II.

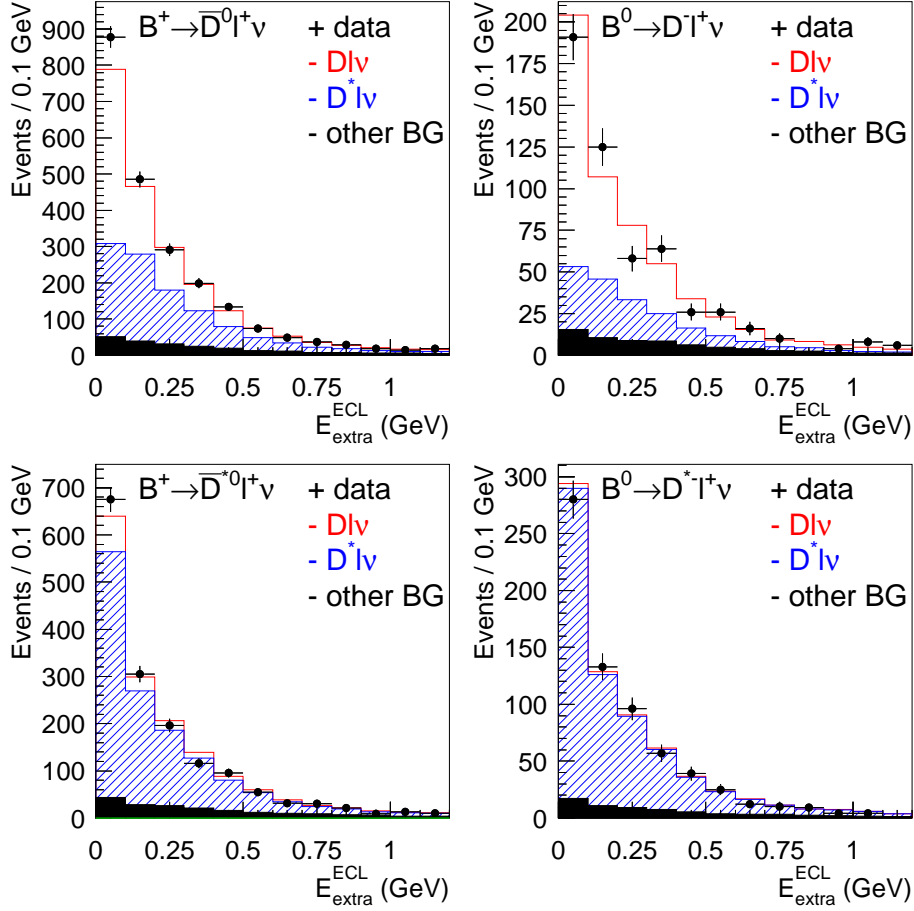


FIG. 2: Comparison of $E_{\text{extra}}^{\text{ECL}}$ distributions for the control samples in data and the MC simulation.

The above procedure to extract the signal yields has been tested by “toy MC experiments”: in each experiment, the number of events in each $(M_{\text{miss}}^2, E_{\text{extra}}^{\text{ECL}})$ bin is generated according to Poisson statistics, with the mean (μ) fixed to the number of events found in the MC simulation, including the $B \rightarrow D^{(*)}\tau\nu$ signals with the SM branching fraction. The distributions are then fit with the procedure described in the previous subsection. We generate 500 experiments, and we confirm that the means of the extracted yields are consistent with the input μ values.

The signal extraction procedure has also been checked by performing a fit to sample distributions from generic MC events, which are the sum of the generic $B\bar{B}$ and $q\bar{q}$ processes, where semileptonic B to τ decays, $B \rightarrow D\tau\nu$, $D^*\tau\nu$ and $D^{**}\tau\nu$, are removed from the $B\bar{B}$ samples. For all four signal decays, the signal yields obtained are consistent with zero within the statistical uncertainty.

6. RESULTS AND SYSTEMATIC UNCERTAINTIES

In this paper, we present a relative measurement; we extract the yields of both the signal mode $\overline{B} \rightarrow D^{(*)}\tau^+\nu$ and the normalization mode $\overline{B} \rightarrow D^{(*)}\ell^+\nu$ to deduce the four ratios,

$$R(\overline{D}^0) \equiv \mathcal{B}(B^+ \rightarrow \overline{D}^0\tau^+\nu)/\mathcal{B}(B^+ \rightarrow \overline{D}^0\ell^+\nu) \quad (4)$$

$$R(\overline{D}^{*0}) \equiv \mathcal{B}(B^+ \rightarrow \overline{D}^{*0}\tau^+\nu)/\mathcal{B}(B^+ \rightarrow \overline{D}^{*0}\ell^+\nu) \quad (5)$$

$$R(D^-) \equiv \mathcal{B}(B^0 \rightarrow D^-\tau^+\nu)/\mathcal{B}(B^0 \rightarrow D^-\ell^+\nu) \quad (6)$$

$$R(D^{*-}) \equiv \mathcal{B}(B^0 \rightarrow D^{*-}\tau^+\nu)/\mathcal{B}(B^0 \rightarrow D^{*-}\ell^+\nu). \quad (7)$$

The yields of the normalization modes are extracted as described in Section 4. For the signal modes, after finalizing the signal selection criteria and completing the studies in previous sections, we have opened the signal region, and performed the fits with the procedure described in Section 5. Figures 3 and 4 show the fit results for $B^+ \rightarrow D^{(*)}\tau\nu$ and $B^0 \rightarrow D^{(*)}\tau\nu$, respectively. There are excesses in the signal region for all four decay modes. Figure 5 shows the signal likelihood curves, while Table IV summarizes the results. The extracted yields (statistical significances) are $98.6^{+26.3}_{-25.0}(4.4)$, $99.8^{+22.2}_{-21.3}(5.2)$, $17.2^{+7.69}_{-6.88}(2.8)$, and $25.0^{+7.17}_{-6.27}(5.9)$, for $B \rightarrow \overline{D}^0\tau^+\nu$, $\overline{D}^{*0}\tau^+\nu$, $D^-\tau^+\nu$ and $D^{*-}\tau^+\nu$, respectively. The efficiency ϵ , shown in Table IV, corresponds to the sum of the signal yields measured in $B \rightarrow D\tau\nu$ and $B \rightarrow D^*\tau\nu$ selections. The ratio of $\mathcal{B}(B \rightarrow D^{(*)}\tau\nu)$ to $\mathcal{B}(B \rightarrow D^{(*)}\ell\nu)$ are calculated as,

$$R(D^{(*)}) = \frac{N(D^{(*)}\tau\nu)}{N(D^{(*)}\ell\nu)} \cdot \frac{2\epsilon(D^{(*)}\ell^+\nu)}{\epsilon(D^{(*)}\tau^+\nu)} \cdot \frac{1}{\mathcal{B}(\tau \rightarrow \ell\nu\nu)}. \quad (8)$$

Note that the efficiency $\epsilon(D^{(*)}\ell\nu)$ is the average over electron and muon modes, while the yields are extracted for the sum of the two modes.

Table V summarizes the systematic errors related to the ratio measurement, where reconstruction efficiency errors are largely cancel out. The following systematic errors are considered.

- M_{miss}^2 **shape:** The systematic error due to uncertainties in the M_{miss}^2 shape is estimated by varying the PDF parameters. The fitting procedure is repeated for each parameter variation, and relative changes in the extracted yields are added in quadrature. This method will give conservative estimates, as there are correlations in M_{miss}^2 resolutions between decay modes.
- $E_{\text{extra}}^{\text{ECL}}$ **shape:** The systematic error due to uncertainties in the $E_{\text{extra}}^{\text{ECL}}$ shape is estimated by varying the content of each PDF histogram bin by its $\pm 1\sigma$ statistical error. The fitting procedure is repeated for each bin variation, and relative changes in the extracted yields are added in quadrature.
- $D^{**}\ell\nu$ **branching fraction:** The systematic errors due to uncertainties in the $\overline{B} \rightarrow D^{**}\ell^+\nu$ component is estimated by varying the branching fraction for each D^{**} component by $\pm 1\sigma$ based on the Belle results in [17]. The relative change in the extracted yields is assigned as the systematic error.

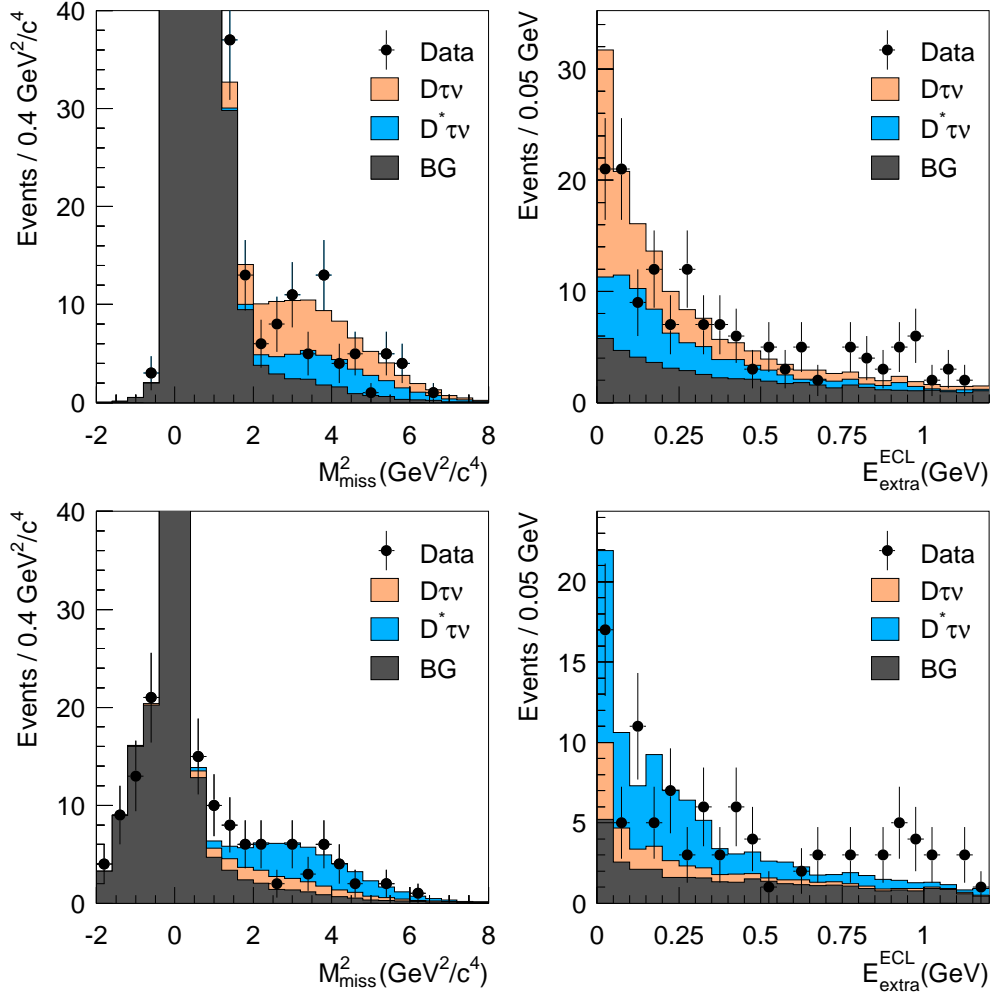


FIG. 3: Fit results for $B^+ \rightarrow \bar{D}^0 \tau^+ \nu$ (top) and $B^+ \rightarrow \bar{D}^{*0} \tau^+ \nu$ (bottom). The M_{miss}^2 (left) and $E_{\text{extra}}^{\text{ECL}}$ (right) distributions are shown with the signal selection cut on the other variable listed in Table I.

- **$D \leftrightarrow D^*$ cross-feed:** In our nominal fitting procedure, the rates of the cross-feed between D and D^* decays are fixed to the values in the MC simulation, for both the signal and normalization decays. The uncertainty is estimated by taking the relative change in the extracted yield for the normalization decays, when the cross-feed component is floated in the fit.
- **$\tau \rightarrow \ell \nu \nu$ branching fraction:** The systematic error due to uncertainties in the branching fraction of τ decay modes is evaluated by changing the branching fractions by the uncertainties in the PDG values [18].

The total systematic error is the quadratic sum of all individual ones.

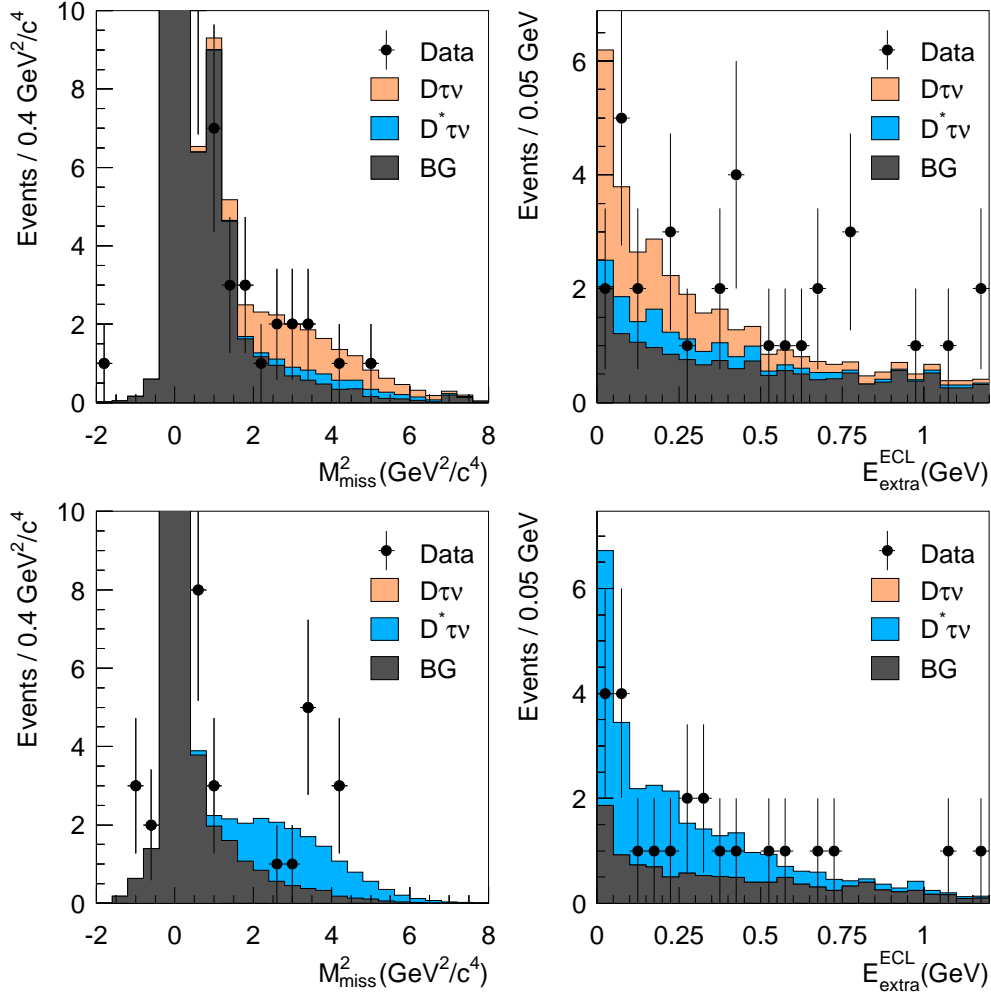


FIG. 4: Fit results for $B^0 \rightarrow D^- \tau^+ \nu$ (top) and $B^0 \rightarrow D^{*-} \tau^+ \nu$ (bottom). The M_{miss}^2 (left) and $E_{\text{extra}}^{\text{ECL}}$ (right) distributions are shown with the signal selection cut on the other variable listed in Table I.

With the systematic errors shown in Table V, the final results for the four ratios are,

$$R(\overline{D}^0) = 0.70 \begin{matrix} +0.19 & +0.11 \\ -0.18 & -0.09 \end{matrix} \quad (9)$$

$$R(\overline{D}^{*0}) = 0.47 \begin{matrix} +0.11 & +0.06 \\ -0.10 & -0.07 \end{matrix} \quad (10)$$

$$R(D^-) = 0.48 \begin{matrix} +0.22 & +0.06 \\ -0.19 & -0.05 \end{matrix} \quad (11)$$

$$R(D^{*-}) = 0.48 \begin{matrix} +0.14 & +0.06 \\ -0.12 & -0.04 \end{matrix} \quad (12)$$

where the first error is the statistical and the second error is the systematic. Including the systematic uncertainties for the yields convolved in the likelihood (Figure 5), the significances of the excesses (in units of σ) are found to be 3.8, 3.9, 2.6 and 4.7 for $B \rightarrow \overline{D}^0 \tau^+ \nu$, $\overline{D}^{*0} \tau^+ \nu$, $D^- \tau^+ \nu$ and $D^{*-} \tau^+ \nu$, respectively.

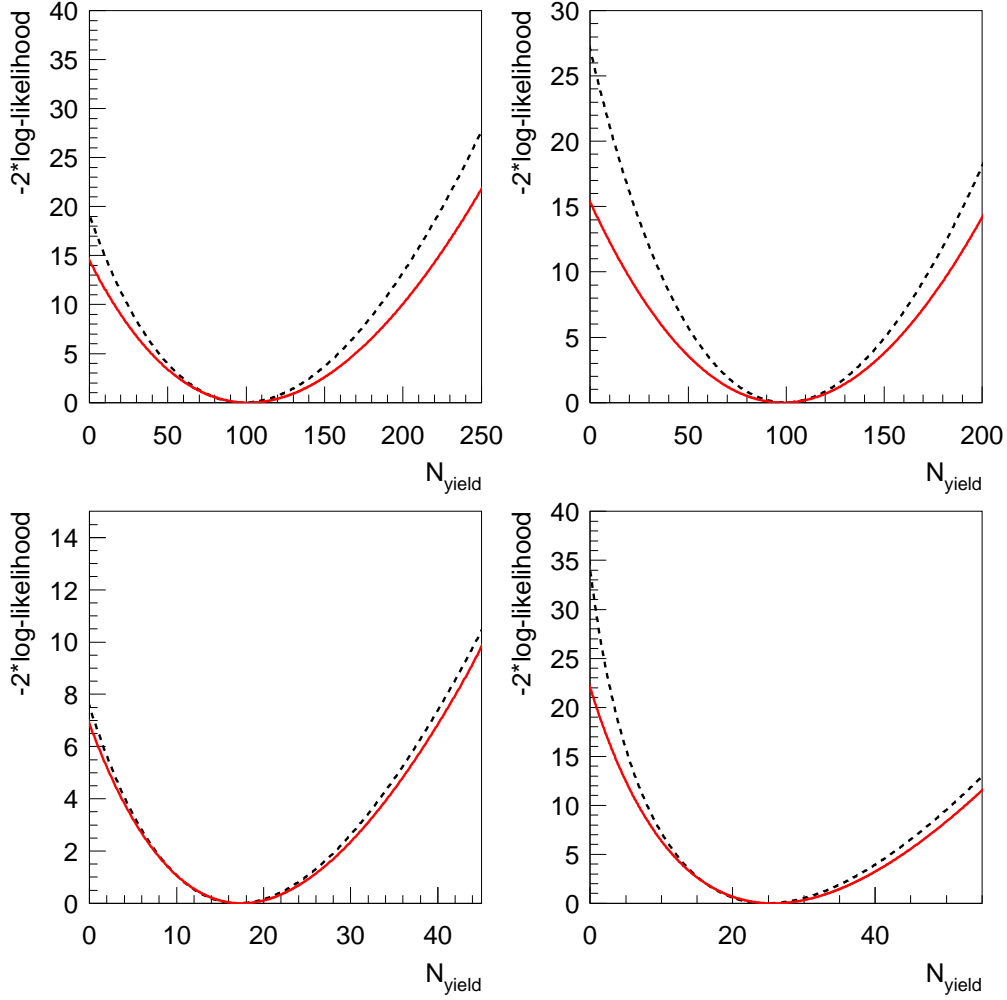


FIG. 5: Likelihood curves as a function of signal yields for $B^+ \rightarrow \bar{D}^0 \tau^+ \nu$ (top-left) and $B^+ \rightarrow \bar{D}^{*0} \tau^+ \nu$ (top-right). $B^0 \rightarrow D^- \tau^+ \nu$ (bottom-left) and $B^0 \rightarrow D^{*-} \tau^+ \nu$ (bottom-right). Red (black) curves show the likelihood with (without) the systematic uncertainty

Using the branching fractions for the $B \rightarrow D^{(*)} \ell \nu$ normalization decays, reported in [18]: $\mathcal{B}(B^+ \rightarrow D \ell \nu) = (2.15 \pm 0.22)\%$, $\mathcal{B}(B^+ \rightarrow D^* \ell \nu) = (6.5 \pm 0.5)\%$, $\mathcal{B}(B^0 \rightarrow D \ell \nu) = (2.12 \pm 0.20)\%$, and $\mathcal{B}(B^0 \rightarrow D^* \ell \nu) = (5.33 \pm 0.20)\%$, we obtain the following branching fractions for $B \rightarrow D^{(*)} \tau \nu$ decays,

$$\mathcal{B}(B^+ \rightarrow \bar{D}^0 \tau^+ \nu) = 1.51^{+0.41}_{-0.39}{}^{+0.24}_{-0.19} \pm 0.15 [\%] \quad (13)$$

$$\mathcal{B}(B^+ \rightarrow \bar{D}^{*0} \tau^+ \nu) = 3.04^{+0.69}_{-0.66}{}^{+0.40}_{-0.47} \pm 0.22 [\%] \quad (14)$$

$$\mathcal{B}(B^0 \rightarrow D^- \tau^+ \nu) = 1.01^{+0.46}_{-0.41}{}^{+0.13}_{-0.11} \pm 0.10 [\%] \quad (15)$$

$$\mathcal{B}(B^0 \rightarrow D^{*-} \tau^+ \nu) = 2.56^{+0.75}_{-0.66}{}^{+0.31}_{-0.22} \pm 0.10 [\%] \quad , \quad (16)$$

where the first error is statistical, the second is systematic, and the third is due to the

Quantity	$\overline{D}^0\tau^+\nu$	$\overline{D}^{*0}\tau^+\nu$
$N(\overline{D}^{(*)}\tau^+\nu)$	$98.6^{+26.3}_{-25.0}$	$99.8^{+22.2}_{-21.3}$
$\epsilon(\overline{D}^{(*)}\tau^+\nu)$ [%]	6.20 ± 0.08	3.86 ± 0.08
R [%]	$70.2^{+18.9}_{-18.0} \text{ }^{+11.0}_{-9.1}$	$46.8^{+10.6}_{-10.2} \text{ }^{+6.2}_{-7.2}$
$\Sigma(\Sigma_{stat})$	3.8 (4.4)	3.9 (5.2)
\mathcal{B} [%]	$1.51^{+0.41}_{-0.39} \text{ }^{+0.24}_{-0.19} \pm 0.15$	$3.04^{+0.69}_{-0.66} \text{ }^{+0.40}_{-0.47} \pm 0.22$
Quantity	$D^-\tau^+\nu$	$D^{*-}\tau^+\nu$
$N(\overline{D}^{(*)}\tau^+\nu)$	$17.2^{+7.7}_{-6.9}$	$25.0^{+7.2}_{-6.3}$
$\epsilon(\overline{D}^{(*)}\tau^+\nu)$ [%]	6.86 ± 0.09	2.09 ± 0.04
R [%]	$47.6^{+21.6}_{-19.3} \text{ }^{+6.3}_{-5.4}$	$48.1^{+14.0}_{-12.3} \text{ }^{+5.8}_{-4.1}$
$\Sigma(\Sigma_{stat})$	2.6 (2.8)	4.7 (5.9)
\mathcal{B} [%]	$1.01^{+0.46}_{-0.41} \text{ }^{+0.13}_{-0.11} \pm 0.10$	$2.56^{+0.75}_{-0.66} \text{ }^{+0.31}_{-0.22} \pm 0.10$

TABLE IV: Summary of the results; extracted yields from the fitting, N , the efficiency to detect the signal in either of $B \rightarrow D\tau(\ell)\nu$ and $B \rightarrow D^*\tau(\ell)\nu$ selections, ϵ , the deduced ratio of $\mathcal{B}(B \rightarrow D^{(*)}\tau\nu)$ to $\mathcal{B}(B \rightarrow D^{(*)}\ell\nu)$, R , significance of the signal with (without) systematic errors, $\Sigma(\Sigma_{stat})$, deduced branching fraction, \mathcal{B} .

Source	$\overline{D}^0\tau^+\nu$ [%]	$\overline{D}^{*0}\tau^+\nu$ [%]	$D^-\tau^+\nu$ [%]	$D^{*-}\tau^+\nu$ [%]
M_{miss}^2 shape	+9.10/-7.89	+9.86/-10.7	+6.39/-5.78	+5.80/-6.12
E_{extra}^{ECL} shape	+10.6/-7.58	+7.01/-9.73	+9.03/-7.27	+9.84/-4.97
$D^{**}\ell\nu$	+0.35/-0.41	+0.75/-0.02	+4.50/-2.56	+0.58/-0.28
$D \leftrightarrow D^*$ cross-feed	+7.05/-6.86	+5.12/-5.34	+5.77/-6.01	+3.48/-3.37
$\mathcal{B}(\tau \rightarrow \ell\nu\nu)$	± 0.3	± 0.3	± 0.3	± 0.3
Total	+15.7/-12.9	+13.2/-15.4	+13.3/-11.4	+12.0/-8.58

TABLE V: Summary of the systematic errors.

branching fraction error of the normalization mode.

7. SUMMARY

Using 604.5 fb^{-1} of data collected at the $\Upsilon(4S)$ resonance with the Belle detector at the KEKB collider, we have measured B to τ semileptonic decays, by fully reconstructing hadronic decays of the accompanying B meson. We have extracted signals for the four decay modes, $B^+ \rightarrow \overline{D}^0\tau^+\nu$, $B^+ \rightarrow \overline{D}^{*0}\tau^+\nu$, $B^0 \rightarrow D^-\tau^+\nu$, and $B^0 \rightarrow D^{*-}\tau^+\nu$, and obtained the branching fractions listed in Section 6. The obtained branching fractions are consistent within errors with the earlier Belle result for $B^0 \rightarrow D^{*-}\tau^+\nu$ [7], and BaBar results for the four signal modes [8]. Our results are slightly higher than the SM expectation, however more luminosity is needed to clarify the deviation.

We thank the KEKB group for the excellent operation of the accelerator, the KEK cryogenics group for the efficient operation of the solenoid, and the KEK computer group and the National Institute of Informatics for valuable computing and SINET3 network support. We acknowledge support from the Ministry of Education, Culture, Sports, Science, and Technology (MEXT) of Japan, the Japan Society for the Promotion of Science (JSPS), and the Tau-Lepton Physics Research Center of Nagoya University; the Australian Research Council and the Australian Department of Industry, Innovation, Science and Research; the National Natural Science Foundation of China under contract No. 10575109, 10775142, 10875115 and 10825524; the Department of Science and Technology of India; the BK21 program of the Ministry of Education of Korea, the CHEP SRC program and Basic Research program (grant No. R01-2008-000-10477-0) of the Korea Science and Engineering Foundation; the Polish Ministry of Science and Higher Education; the Ministry of Education and Science of the Russian Federation and the Russian Federal Agency for Atomic Energy; the Slovenian Research Agency; the Swiss National Science Foundation; the National Science Council and the Ministry of Education of Taiwan; and the U.S. Department of Energy. This work is supported by a Grant-in-Aid from MEXT for Science Research in a Priority Area (“New Development of Flavor Physics”), and from JSPS for Creative Scientific Research (“Evolution of Tau-lepton Physics”).

-
- [1] C.-H. Chen and C.-Q. Geng, *J. High Energy Phys.* **10**, 053 (2006).
 - [2] B. Grzadkowski and W.-S. Hou, *Phys. Lett. B* **283**, 427 (1992).
 - [3] M. Tanaka, *Z. Phys. C* **67**, 321 (1995).
 - [4] K. Kiers and A. Soni, *Phys. Rev. D* **56**, 5786 (1997).
 - [5] H. Itoh, S. Komine and Y. Okada, *Prog. Theor. Phys.* **114**, 179 (2005).
 - [6] Ulrich Nierste, Stephanie Trine, Susanne Wesoff, arXiv:0801.4938.
 - [7] A. Matyja, M. Rozanska *et al.* (Belle Collaboration), *Phys. Rev. Lett.* **99**, 191807 (2007).
 - [8] B. Aubert *et al.* (BaBar Collaboration), *Phys. Rev. Lett.* **100**, 021801 (2008); B. Aubert *et al.* (BaBar Collaboration), *Phys. Rev. D* **79**, 092002 (2009).
 - [9] S. Kurokawa and E. Kikutani, *Nucl. Instr. and Meth. A* **499**, 1 (2003), and other papers included in this volume.
 - [10] A. Abashian *et al.* (Belle Collab.), *Nucl. Instr. and Meth. A* **479**, 117 (2002).
 - [11] R. Brun *et al.*, GEANT3.21, CERN Report DD/EE/84-1 (1984).
 - [12] See the EvtGen package home page, <http://www.slac.stanford.edu/~lange/EvtGen/>.
 - [13] D. Scora and N. Isgur, *Phys. Rev. D* **52**, 2783 (1995).
 - [14] C. Fox and S. Wolfram, *Phys. Rev. Lett.* **41**, 1581 (1978).
 - [15] H. Albrecht *et al.*, (ARGUS Collaboration), *Phys. Lett. B* **185**, 218 (1987).
 - [16] E.D. Bloom and C. Peck, *Annu. Rev. Nucl. Part. Sci.* **33**, 143 (1983).
 - [17] D. Liventsev *et al.* (Belle Collaboration), *Phys. Rev. D* **77**, 091503(R) (2008).
 - [18] W.-M. Yao *et al.* (Particle Data Group), *J. Phys. G* **33**, 1 (2006).